

## Capillary nematization of colloidal rods in confinement

Kira E. Klop<sup>a</sup>, Roel P. A. Dullens<sup>a</sup>, M. Paul Lettinga<sup>b, c</sup>, Sergei A. Egorov<sup>d</sup>, and Dirk G. A. L. Aarts<sup>a</sup>

<sup>a</sup>Department of Chemistry, Physical and Theoretical Chemistry Laboratory, University of Oxford, Oxford, OX1 3QZ, UK; <sup>b</sup>Institut für Informatik, Albert-Ludwigs-Universität, Freiburg, Germany; <sup>c</sup>Laboratory for Soft Matter and Biophysics, KU Leuven, Celestijnenlaan 200D, B-3001 Leuven, Belgium; <sup>d</sup>Department of Chemistry, University of Virginia, Charlottesville, VA 22901, USA

### ARTICLE HISTORY

Compiled May 31, 2018

### ABSTRACT

We confine a colloidal liquid crystal between parallel plates separated down to several times the rod length. By connecting the system to a air we effectively create a grand-canonical system, in which the liquid crystal displays an isotropic phase in the reservoir, but upon strong confinement becomes nematic between the parallel plates. This capillary nematization transition can be followed down to the single particle level by means of laser scanning confocal microscopy. We compare the experimental findings to density functional theories, within the Zwanzig model as well as a more advanced density functional theory, in which the effect of rod flexibility is taken into account.

### KEYWORDS

Colloids; Liquid Crystals; Capillarity; Wetting

## 1. Introduction

Hard rod-like particles, which are governed by entropy alone, display rich liquid crystalline phase behavior [1]. The confinement of liquid crystals leads to even more complex phenomena: its study is of ongoing interest both from a fundamental point of view, to obtain a better understanding of the interplay between bulk properties and wall-induced effects, and for applications such as LCDs, where there is an ongoing trend towards smaller cells. Recently, interest in lyotropic liquid crystals in confinement has greatly increased, leading to theory [2–4], experiments [2, 5–7] and simulations [8–10] in order to better understand effects of confinement, where LC-wall interactions lead to different behavior than in bulk.

Lyotropic liquid crystals are particularly interesting as a model system for biological processes, as many of the cell structures, e.g. membranes and filaments, exhibit liquid crystalline properties [11, 12]. As a cell is a very small and crowded environment, the phase behavior of many of these structures will be affected by confinement [13]. It has been shown, for example, that cytoskeletal filaments will form bundles due to

confinement and, in mixtures of filaments, will segregate based on the flexibility of the different filaments [14, 15].

Here, we study the isotropic phase of a colloidal liquid crystal in confinement and particularly focus on the capillary nematization phenomenon, where the confined nematic phase becomes stable at a concentration below the bulk isotropic-nematic phase coexistence, similar to capillary condensation in simple fluids. When rods in an isotropic phase are confined between walls, it becomes entropically favorable to align their major axis along the walls, increasing the accessible space. This leads to a positive adsorption of the rods at each wall forming a nematic layer, despite the overall concentration being below the isotropic-nematic transition in bulk. When the distance between walls is sufficiently small even an isotropic-to-nematic phase transition throughout the sample may be observed. This phenomenon was first predicted by Sheng [16] and later by Poniewierski and Sluckin [17]. Capillary nematization has experimentally been confirmed for thermotropic liquid crystals, where the phase transition was inferred from the force profile originating from confining a molecular liquid crystal between a wall and a colloidal sphere attached to an atomic force microscope [18]. For lyotropic liquid crystals, capillary nematization has been studied in theory and simulations, see e.g. [4, 19–26], however, direct experimental visual confirmation of capillary nematization for lyotropic liquid crystals has not yet been reported.

In this paper we experimentally show a capillary nematization transition in a colloidal liquid crystal, using dispersions of *fd*-virus particles in microfluidic channels of different heights. We observe a clear capillary transition in qualitative agreement with density functional theory (DFT) calculations based on the Zwanzig model, in which rods can only have three different directions. A more advanced density functional theory, in which rods may point along any direction and in which the flexibility of the rods has been taken into account, shows more quantitative agreement to the experiments. The theoretical predictions furthermore shine light on the possibility of experimentally observing adsorption phenomena at single walls.

## 2. Experiments

We dispersed *fd*-virus particles, grown using standard methods described in [27], in 20 mM TRIS-HCl buffer at pH 8.2 with 100 mM NaCl and 15% ethanol. These virus particles are rod-shaped, with a length of 880 nm, a diameter of 6.6 nm and a persistence length of 2200 nm, and are commonly used as a model system for liquid crystals [28–33]. The isotropic phase was isolated from an isotropic-nematic biphasic system and then either used as such, or diluted to 90% (w/w) or 99.5% (w/w) of the coexistence concentration of the isotropic phase in bulk ( $c_I$ ), depending on the experiment. This was done to ensure that the sample is completely isotropic in bulk, yet very close to the bulk isotropic-nematic phase transition, so that capillary nematization can be achieved with a relatively small degree of confinement. A small portion of the virus particles was fluorescently labelled with Alexa-488 NHS ester. The samples were studied with laser scanning confocal microscopy (LSCM) using a Zeiss LSM 5 Exciter, 63x 1.4 NA oil-immersion objective.

Microfluidics channels with different heights between 1  $\mu\text{m}$  and 12  $\mu\text{m}$  (roughly 1.1 – 13.6  $L$ , where  $L$  is the length of a rod) and either a width of 560  $\mu\text{m}$  and a length of 7 mm or a width of 300  $\mu\text{m}$  and a length of 18 mm, were created in NOA81 UV glue using the method described in [34]. In the case of 7 mm long channels, each channel was then placed in a glass vial, such that the vial acts as a reservoir from which particles

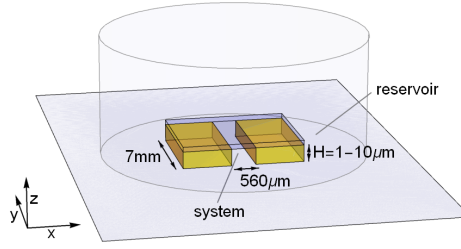


**Figure 1.** Schematic representation of the sample cell. The micro-channel itself is in between the two yellow blocks, which represent UV glue. The channel is closed on both top and bottom by a coverslip, and the entire channel is enclosed in a small glass vial, glued onto the bottom coverslip.

can freely enter or leave the channel, effectively creating a grand canonical system. A schematic representation of this grand canonical sample cell is shown in figure 1. The addition of a reservoir is necessary for capillary nematization to occur, as the phase transition leads to an increase of the rod concentration inside the channel, which can only occur if there is a reservoir of rods, from which particles can be drawn into the channel. The 18 mm long channels were sealed at both ends after adding the sample, creating a canonical system with effectively a finite reservoir as explained in the next paragraph.

The channels were plasma-cleaned and subsequently filled via capillary action by adding approximately 50  $\mu\text{L}$  of the sample per channel (“grand canonical”) or 2  $\mu\text{L}$  per 9 channels (“canonical”) to one end of the channel(s). Only a very small amount of sample was required to fill the channel, and in the case of the grand canonical system, the rest of the sample was left at the end of the channel (but inside the glass vial) and acted as a particle reservoir. In the canonical system, the channels were sealed at both ends using UV glue after filling the channels. Although these channels do not have a well-defined reservoir, the amount of sample used was larger than what is required to fill the channel, and therefore the excess fluid may act as a finite (small) reservoir, of which the volume can be estimated experimentally. We found no signs of particles sticking to the confining walls.

LSCM images were recorded for the samples in channels of different heights in order to determine the phase behavior. Time series were recorded in the  $xy$ -plane at  $z = 0$ , halfway in height between the two confining walls, such that any nematic phase seen must be a capillary nematic state, and not adsorption at each wall. In order to see whether adsorption happens at the confining walls in the experiment, LSCM images were recorded at different heights throughout a channel, with a distance of  $\Delta z = 0.2 \mu\text{m}$  (i.e.  $0.23 L$ ) between frames.

### 3. Results

#### 3.1. Grand-canonical system

The isotropic phase taken from a biphasic sample was diluted to 99.5% (w/w), to ensure that the sample is completely isotropic in bulk. Channels with heights of 2.0, 5.1, 6.7 and 10.8  $L$  were used in these experiments.

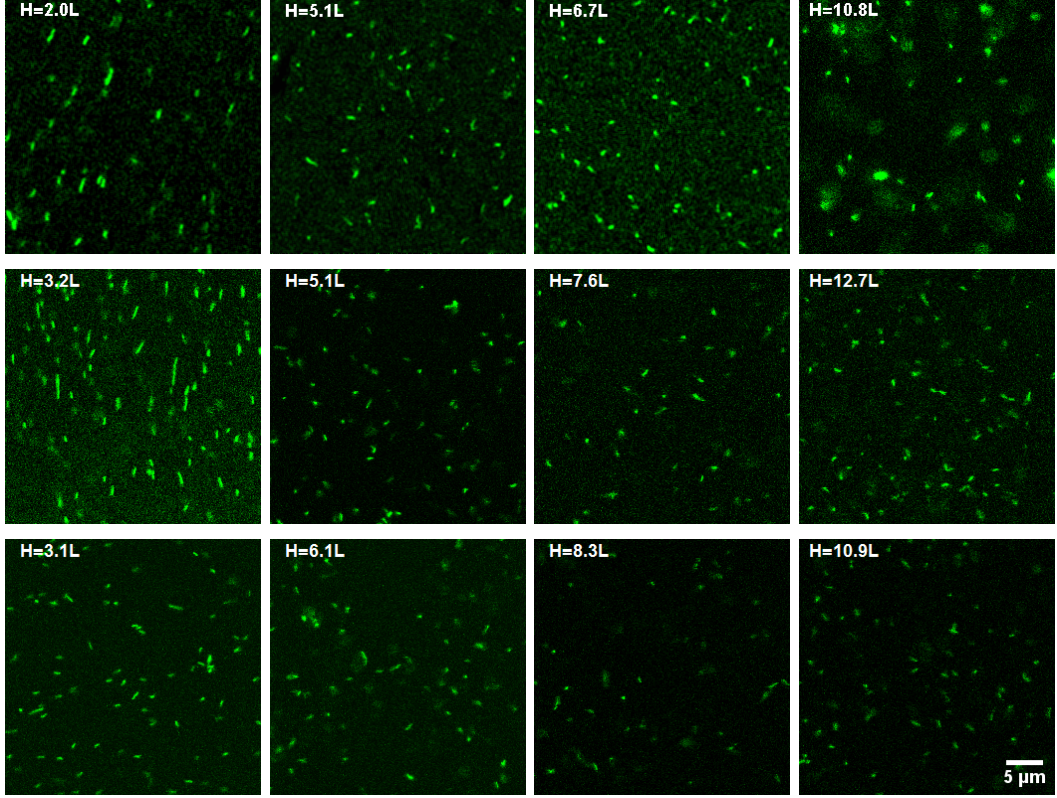


**Figure 2.** LSCM images of *fd*-virus particles in microfluidics channels of different heights. Top: grand canonical system,  $c = 0.995c_I$ . Each image is a superposition of 5 frames, to increase the number of particles per frame. Middle: canonical system,  $c = c_I$  and bottom: canonical system,  $c = 0.9c_I$ .

The top row in figure 2 shows typical LSCM images recorded in the middle of a channel ( $z = 0$ ) for each of the channel heights used. The sample remains isotropic down to a confinement of  $5.1 L$ . However, when confined to channel with wall-to-wall separation of  $2.0 L$ , the particles become aligned and the system displays a nematic phase. No adsorption at the walls was seen in any of the isotropic samples.

In order to quantify the results, the order parameter  $S$  was calculated for each sample using

$$S = 2 \langle \cos^2 \theta' \rangle - 1, \quad (1)$$

where  $\theta'$  is the orientation of a particle projected on the  $xy$ -plane, as we measure it from our confocal images, with respect to the average projected orientation of all particles in that frame. Because we can only measure this projected angle, and not the full 3D angle, the order parameter equivalent to that of a 2D system should be used, which has been shown to be a good estimate of the 3D order parameter [35].

The order parameter for each time series, recorded in the middle of the channel in terms of height, was calculated. As there are relatively few particles per frame, particles from 10 independent frames were combined before calculating the order parameter, leading to an average of 200 or more tracked particles per calculation. This was done for at least 5 time series of 10 frames and then averaged for each channel height. The result is shown in figure 3(a). The order parameter for the channel with  $H = 2.0 L$  was found to be 0.73, which is clearly much higher than the order parameter found in the bigger

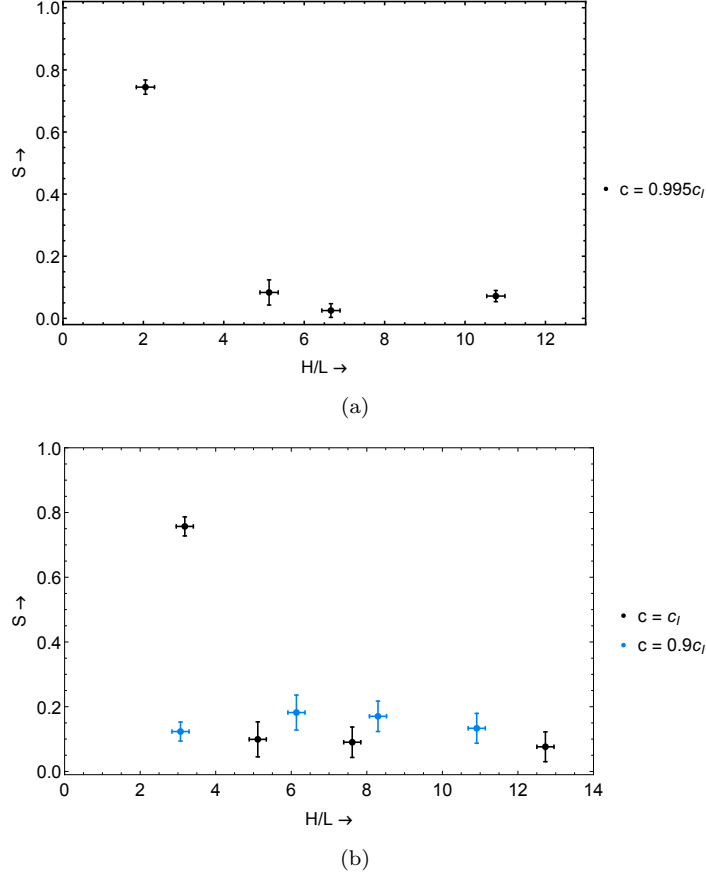


**Figure 3.** Order parameter in (a) the grand canonical system and (b) the canonical system, plotted versus the height of the channel. Error bars represent the standard deviation.

channels, which was typically around 0.1. This indicates that capillary nematization has indeed occurred in the smallest channel. The order parameter calculated for LSCM images recorded at different heights in a channel was not found to change significantly throughout the channel for any of the channel heights.

### 3.2. Canonical system

Experiments in the canonical system were performed to study the effect of concentration on capillary nematization. The experiments were done in a canonical system simply because they were performed before the grand canonical system was designed. The isotropic phase isolated from a biphasic sample was either used as such, or diluted to 90% of the original concentration. Different channel heights between  $2\text{ }\mu\text{m}$  to  $12\text{ }\mu\text{m}$  ( $2.3 - 13.6\text{ }L$ ) were used in these experiments. Due to the nature of the channel fabrication process, the channels used are not exactly the same height for both samples.

The middle ( $c = c_I$ ) and bottom ( $c = 0.9c_I$ ) rows of figure 2 shows typical LSCM images recorded in the middle of a channel ( $z = 0$ ) for each of the channel heights used. It can be seen that the sample is isotropic in all cases except for the higher concentration sample in a channel of  $3.2\text{ }L$ , where the particles are more aligned. As with the grand canonical sample, no adsorption into a nematic layer was seen in any

of the isotropic samples.

The order parameter  $S$  was calculated for each image series, taken in the centre of a channel in terms of height, using equation 1. The resulting order parameters are shown in figure 3(b). The order parameter was found to be 0.76 in the channel, in which the capillary nematization had occurred, and around 0 to 0.2 for the other channels. As with the grand canonical system, the order parameter was not found to change significantly at different heights throughout a channel.

The fact that capillary nematization occurs in the smallest channel for a sample with a concentration of the isotropic phase at coexistence, but not in the sample which was diluted to 90% indicates that it is indeed capillary nematization, and not for example a filling effect of the smaller channels that aligned the rods along the direction of the channel. The sample stayed isotropic in the bigger channels even for a concentration at coexistence, which is an indication that we indeed have a finite-sized reservoir.

### 3.3. DFT within the Zwanzig model

We will now first compare our results to theoretical calculations using DFT within the Zwanzig model [36]. This is one of the simplest models in which rods are considered to be rectangular blocks of  $L \times D \times D$ , with  $L \gg D$ , that can only be oriented along one of three perpendicular unit vectors  $\hat{x}_i$ . This model has been shown to give qualitatively accurate results for the isotropic-nematic transition [36] and confinement phenomena [19, 20] of hard rods. Although calculations for the capillary nematization transition have been performed previously using the Zwanzig model, here we calculate the phase diagram corresponding to our exact system, using the dimensions of rods and confinement used in the experiments.

We base our Zwanzig calculations on a paper by van Roij et al. [20], where the equilibrium phase behavior for Zwanzig rods confined between two parallel plates is calculated in a grand canonical ensemble by minimizing the grand potential function  $\Omega(c)$ , where  $c = L^2 D \rho$  is the dimensionless number density, with  $\rho$  the actual number density. Each of the three possible orientations  $\hat{x}_i$  is considered to be a different chemical species, with number densities  $c_i(z)$ , where  $z$  is the direction perpendicular to the confining walls, with  $z = 0$  being at the center of the channel. A hard wall-rod interaction is incorporated as external potentials  $V_i(z)$  and the separation between the two walls is  $H$  in units of particle length.

The grand potential function for this system is given by

$$\begin{aligned} \frac{\beta \Omega(c) L^2 D}{A} = & \sum_{i=1}^3 \int dz c_i(z) (\log c_i(z) - 1 - \beta \mu(c_R) \\ & + \beta V_i(z)) + 2 \int dz (c_1(z) c_2(z) \\ & + (c_1(z) + c_2(z)) \bar{c}_3(z)), \end{aligned} \quad (2)$$

where  $\beta = 1/k_B T$ ,  $\bar{c}_i(z) = \frac{1}{L} \int_{z-L/2}^{z+L/2} dz' c_i(z')$  and  $\mu(c_R)$  the chemical potential, with  $c_R$  the concentration of rods in the particle reservoir. The Euler-Lagrange equations, obtained from the minimization conditions  $\partial \Omega(c) / \partial c_i(z) = 0$ , are solved iteratively to obtain the equilibrium particle densities  $c_i(z)$ . In order to simulate a finite reservoir,  $c_R$  and  $\mu$  are re-evaluated at each iterative step, based on the total particle density inside the channel,  $c$ , and the starting reservoir concentration  $c_{R,0}$ , assuming the volumes of reservoir and channel are constant. The total volume  $V_{tot}$ , of reservoir and channel

together, was set to (i) 50  $\mu\text{L}$ , in agreement with the grand canonical experiments, or (ii) 2  $\mu\text{L}/9$  channels  $\approx 0.22$   $\mu\text{L}$  (for each channel), which was approximately added to each channel in the canonical systems before sealing them. Note that for (i) the reservoir is much larger than the channel, such that the iterative steps only change the concentration of the reservoir by a small amount.

The total concentration of rods  $c(z)$  and orientational order parameters  $s(z)$  and  $\Delta(z)$  were then calculated using

$$\begin{aligned} c(z) &= c_1(z) + c_2(z) + c_3(z), \\ s(z) &= \frac{c_3(z) - \frac{1}{2}(c_1(z) + c_2(z))}{c(z)}, \\ \Delta(z) &= \frac{c_1(z) - c_2(z)}{c(z)}. \end{aligned} \tag{3}$$

The order parameters are chosen such that for an isotropic phase  $s(z) = \Delta(z) = 0$ , and for a perfect nematic phase with the director parallel to the walls  $\Delta(z) = \pm 1$  and  $s(z) = -\frac{1}{2}$ . For a more detailed discussion of these two order parameters the reader is referred to [20]. Note that the experimental order parameter  $S$  should be compared to  $\Delta(z)$ , not  $s(z)$ .

The average concentration inside the channel,  $c = \frac{1}{H} \int_{-H/2}^{H/2} dz c(z)$ , was calculated for many different starting concentrations  $c_{R,0}$  and wall separations  $H$ . The phase diagrams shown in figure 4 were created by plotting  $c$  against  $c_R$  for each of these calculations. Each line in the phase diagram corresponds to a different wall separation  $H$ . In both phase diagrams, a capillary nematization transition occurs for approximately  $H \gtrsim 2L$  at a certain value of  $c_R$ , where the concentration inside the channel jumps to a higher value. Note that due to our iterative scheme the density jumps do not exactly match the binodal points, but we find a jump in between the two spinodal points, which is a small shift from the actual phase transition. From calculations of the order parameters we confirmed that the jumps are indeed between an isotropic and a nematic phase. For smaller  $H$  there is no phase transition visible, as in this case the sample inside the channel will be nematic even at very low  $c_R$ . The difference between the two phase diagrams is most obvious in the difference in concentration,  $c$ , between the isotropic and capillary nematic phases, which is much smaller for the smaller reservoir size. In addition, a higher  $c_R$  is required for capillary nematization to occur in the smaller reservoir size for the same wall-to-wall distance  $H$ . Both of these differences can be explained by the fact that for a smaller reservoir, a small change in concentration due to particles from the reservoir entering the channel when capillary nematization occurs, will have a larger impact on the concentration of particles in the reservoir itself.

In the experiments we used a starting reservoir concentration that was 90%, 99.5% or 100% of the concentration of a bulk isotropic phase in coexistence with its nematic phase. In the DFT within the Zwanzig model the isotropic phase in coexistence with a nematic phase has a concentration of  $c_I = 1.258$  [20]. The experimental concentrations therefore correspond to  $c_{R,0} = 1.132, 1.252$  and  $1.258$  respectively in the Zwanzig model. The experimental reservoir concentrations are indicated in figure 4 with dashed vertical lines.

It can be seen that for the grand canonical system (figure 4(a)) at the experimental concentration, capillary nematization is expected to occur for  $H \lesssim 4.7L$ . Given the approximate nature of the model this corresponds remarkably well with our experi-

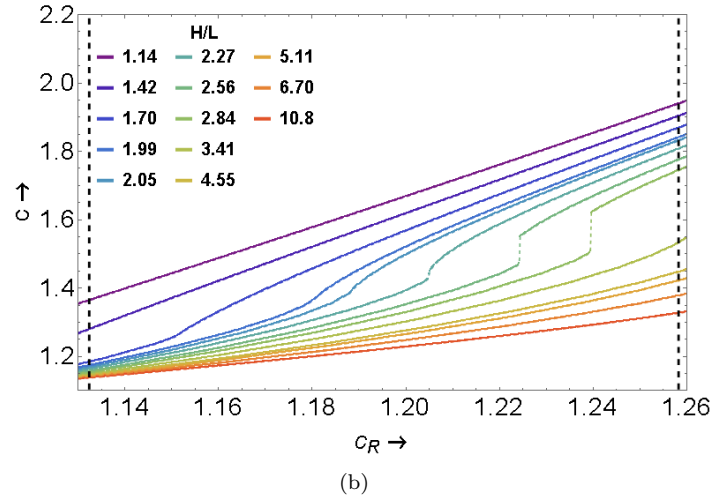
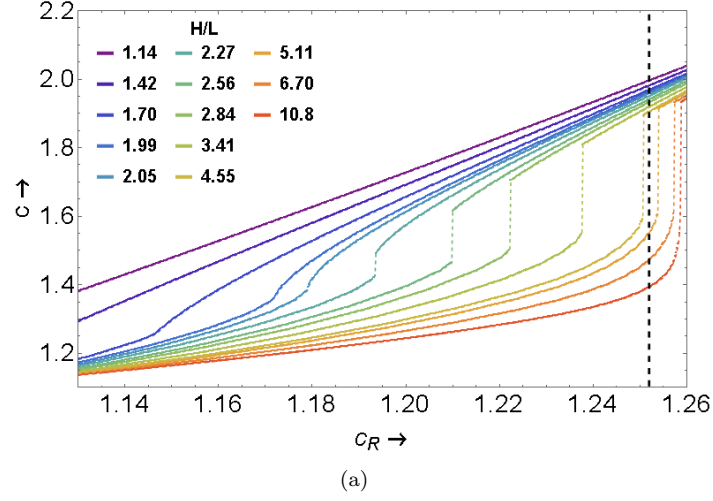


**Figure 4.** Phase diagrams calculated using DFT within the Zwanzig model for (a)  $V_{tot} = 50 \mu\text{L}$ , as used in the grand canonical system, and (b)  $V_{tot} \approx 0.22 \mu\text{L}$ , as estimated for the canonical system. Each line represents a different channel height  $H$ . Plotted is the density inside the channel versus the density in the reservoir. The vertical dashed lines indicate the reservoir concentrations used in the experiments.



ments, where we found capillary nematization to occur in a channel with  $H = 2.0 L$ , but not in a channel with  $H \geq 5.1 L$ . In the case of the canonical system (figure 4(b)) capillary nematization occurs at  $H \lesssim 3.3 L$  for the undiluted sample, and at  $H \lesssim 1.5 L$  for the sample diluted to 90%. Again, this corresponds very well with our experiments, where we observe a phase transition between  $H = 3.2 L$  and  $H = 5.1 L$  for the undiluted sample, and do not observe capillary nematization in any channel heights down to  $H = 3.1 L$  for the diluted sample.

The order parameter in the center of the channel, at  $z = 0$ , was calculated for different wall separations in order to compare this to our experimental order parameters. Again, the transition can clearly be seen, see figure 5. However, the exact value of the order parameter shows a discrepancy between experiment and Zwanzig theory. It is possible that this discrepancy is caused by the relative simplicity of the model, where only three orientations are allowed and the flexibility of rods is not taken into account. We therefore performed additional DFT calculations for orientationally unrestricted semiflexible chains, recently developed specifically to study *semiflexible* polymers confined between flat walls [37].

### 3.4. DFT for orientationally unrestricted semiflexible chains

The two key novel features of this alternative DFT approach, which distinguish it from the Zwanzig model discussed above, are (1) the *finite flexibility* of the rods (incorporated in the microscopic model via the stiffness parameter of the bond-bending potential), and (2) the *unrestricted* angular orientations of the rods (achieved by implementing DFT in continuous space). While it is clearly crucial to account for the finite flexibility of the *fd*-virus particles used in the experiments, the unrestricted orientation is equally important for the present problem, since orientationally restricted treatments of capillary nematization are known to suffer from artefacts [22]. Accordingly, it is of interest to compare the results of this new DFT method both with the Zwanzig DFT and the experiment.

In brief, our microscopic description of a semiflexible rod is based on a tangent hard-sphere model augmented with a bond-bending potential, whose stiffness parameter directly determines the persistence length of the linear chain (in our calculations we set the persistence length to be roughly 3 times the contour length to mimic the *fd*-virus parameters). The confinement is modeled via two hard flat parallel walls (in *xy*-planes, separated by distance  $H$  along the *z*-axis). As usual, the DFT approach is based on minimizing the free energy of the system and produces the equilibrium density distribution, which is both spatially and orientationally inhomogeneous. By integrating over the angular variables, one obtains the order parameter of the system  $S(z)$  as a function of the distance from the confining walls. The relevant DFT equations and the details of the numerical implementation are provided in Ref. [37]. Furthermore, differences and similarities between the present model of semiflexible chains and those used in earlier theories have been discussed extensively in [38].

Our DFT results for the value of the order parameter in the middle of the slit, at  $z = 0$ , are shown in figure 5(a) together with the experimental data. Note that the DFT calculations were only calculated grand canonically and thus only compared to the experiments with the large reservoir. One observes fairly good agreement in terms of the slit height value where the capillary nematization takes place. Furthermore, both DFT and experiment produce small but non-zero values of  $S$  for the slit heights significantly higher than the one corresponding to the nematization. On the theory

side, this behaviour is due to the residual propagation of the wall-induced order all the way towards the middle of the slit. Overall the novel orientationally unrestricted DFT based on a semiflexible chain model produces the values of the order parameter in the middle of the slit (as a function of the slit height) that are in good agreement with the experimental observations.

The incorporation of non-restricted orientation and rod flexibility clearly makes a large difference in the nature of the capillary nematization transition and the order parameter values found. We refer the reader to recent work by Luzhbin and Chen [26], who show that the flexibility of rods indeed has a significant influence on the (nature of the) transition.

Apart from capillary nematization itself, both the Zwanzig theory and the DFT calculations performed for orientationally unrestricted semiflexible chains reveal that nematic ordering also appears in the vicinity of the walls well before the capillary nematization transition has taken place, see figure 6(c) and 6(d). The Zwanzig model predicts a pronounced nematic layer, whereas the more advanced DFT calculations show that the region of increased concentration is much thinner, although the increased ordering continues for several rod lengths away from the walls.

As discussed earlier, no nematic layers were seen in the experiments. One possible explanation for this could be that the thickness of the adsorbed layer is smaller than the axial resolution of the confocal microscope, and therefore cannot be resolved.

#### 4. Conclusion

In conclusion, we have experimentally shown capillary nematization in a colloidal liquid crystal, which, to the best of our knowledge, has not been observed before. We have compared our results with DFT calculations using both the Zwanzig model for restricted rigid rods and a model of orientationally unrestricted semiflexible chains, and find very good agreement for capillary nematization itself. The adsorbed nematic layers predicted by theory were not observed in any of the experiments.

#### Acknowledgements

This work was supported by the European Research Council [Advanced Grant 291234 (MiCE)].

#### References

- [1] P. Bolhuis and D. Frenkel, *J. Chem. Phys.* **106**, 666 (1997).
- [2] A.H. Lewis, I. Gârlea, J. Alvarado, O.J. Dammone, P.D. Howell, A. Majumdar, B.M. Mulder, M.P. Lettinga, G.H. Koenderink and D.G.A.L. Aarts, *Soft Matter* **10**, 7865–7873 (2014).
- [3] R.M.W. van Bijnen, R.H.J. Otten and P. van der Schoot, *Phys. Rev. E* **86**, 051703 (2012).
- [4] R. Aliabadi, M. Moradi and S. Varga, *Phys. Rev. E* **92**, 032503 (2015).
- [5] O.J. Dammone, I. Zacharoudiou, R.P.A. Dullens, J.M. Yeomans, M.P. Lettinga and D.G.A.L. Aarts, *Phys. Rev. Lett.* **109**, 108303 (2012).
- [6] Y. Geng, D. Seč, P.L. Almeida, O.D. Lavrentovich, S. Žumer and M.H. Godinho, *Soft Matter* **9**, 7928–7933 (2013).

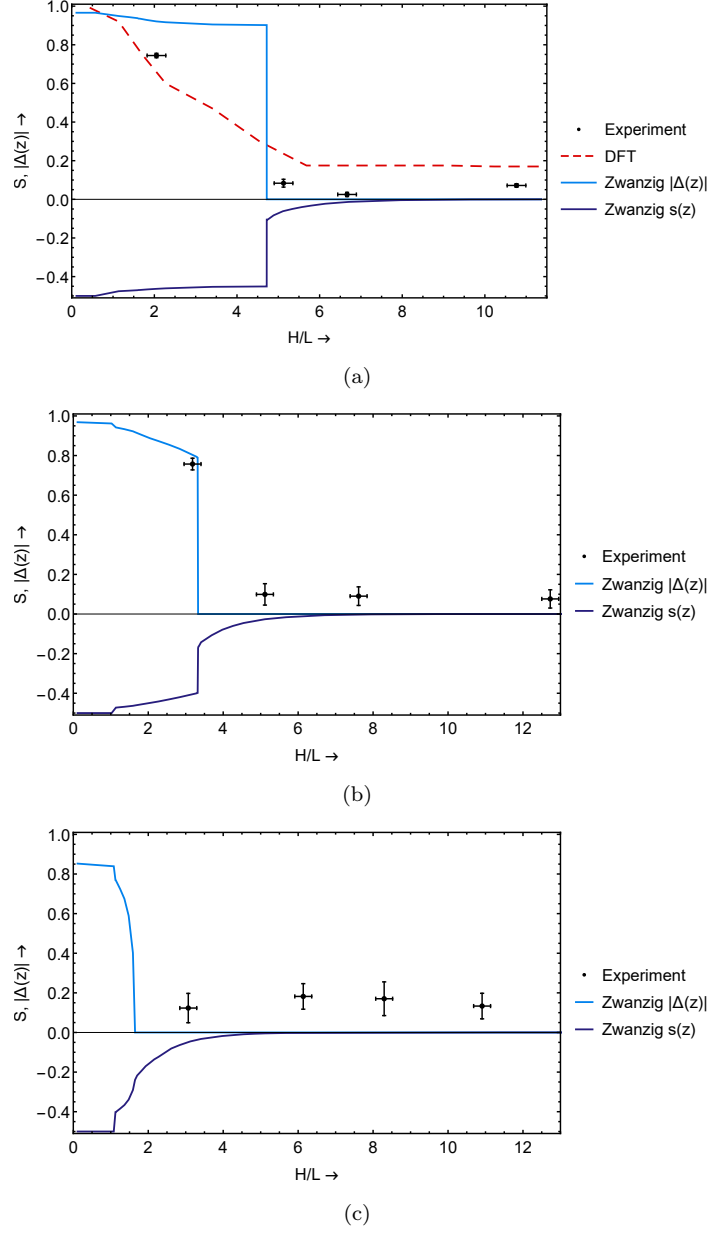


**Figure 5.** Order parameter of the sample versus the height of the channel and corresponding results from DFT calculations and the Zwanzig model. Calculated for (a) the grand canonical system, (b) the canonical system at  $c = c_I$  and (c) the canonical system at  $c = 0.9c_I$ . Error bars represent the standard deviation.

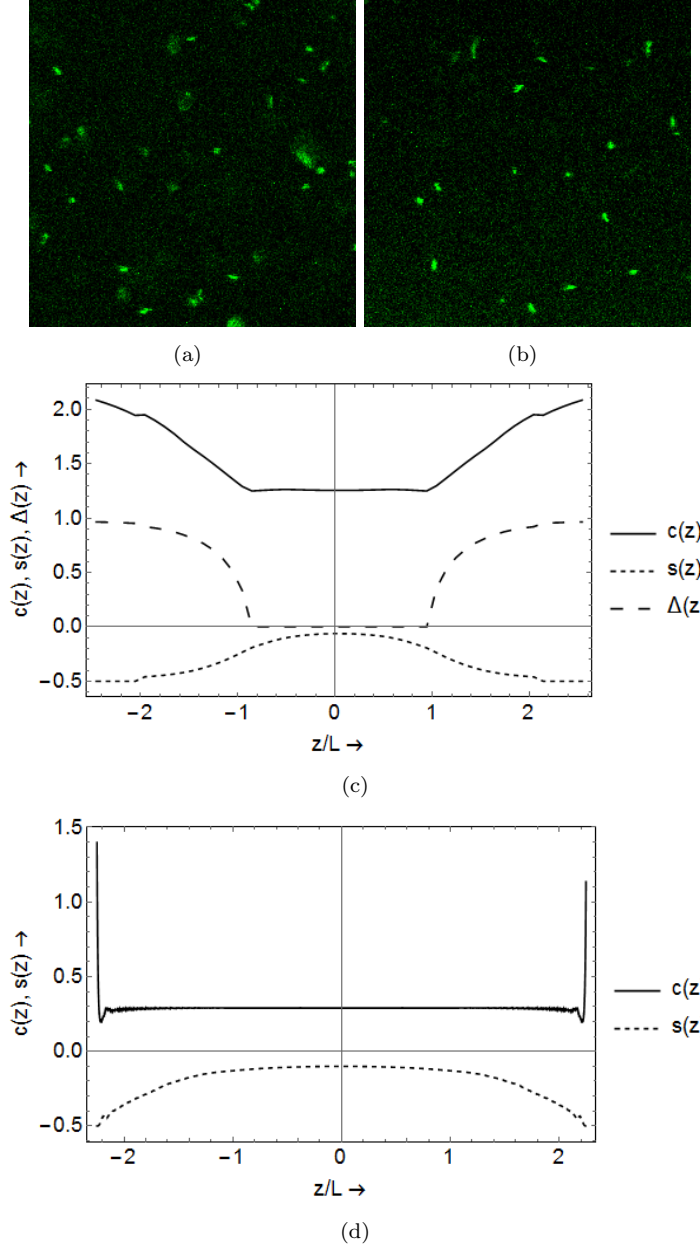


**Figure 6.** (a) Concentration  $c(z)$  and order parameters  $s(z)$  and  $\Delta(z)$  for a channel of  $H/L = 4.5$  calculated using the DFT Zwanzig theory and (b) concentration  $c(z)$  and order parameter  $S(z)$  for a channel of  $H/L = 4.5$  calculated using the more elaborate DFT for orientationally unrestricted semiflexible chains. Both were calculated using the parameters of the grand canonical system.

- [7] I. Gârlea, P. Mulder, J. Alvarado, O.J. Dammone, D.G.A.L. Aarts, M.P. Lettinga, G.H. Koenderink and B.M. Mulder, *Nature Comm.* **7**, 12112 (2016).
- [8] M.L. Blow, S.P. Thampi and J.M. Yeomans, *Phys. Rev. Lett.* **113**, 248303 (2014).
- [9] S. Dussi, S. Belli, R. van Roij and M. Dijkstra, *J. Chem. Phys.* **142** (2015).
- [10] T. Geigenfeind, S. Rosenzweig, M. Schmidt and D. de las Heras, *J. Chem. Phys.* **142**, 174701 (2015).
- [11] M. Soares e Silva, J. Alvarado, J. Nguyen, N. Georgoulia, B.M. Mulder and G.H. Koenderink, *Soft Matter* **7**, 10631–10641 (2011).
- [12] A.D. Rey, *Soft Matter* **6**, 3402–3429 (2010).
- [13] J. Alvarado, B.M. Mulder and G.H. Koenderink, *Soft Matter* **10**, 2354–2364 (2014).
- [14] D.T. Kulp and J. Herzfeld, *Biophysical Chemistry* **57**, 93 – 102 (1995).
- [15] J. Herzfeld, *J. Molecular Recognition* **17**, 376–381 (2004).
- [16] P. Sheng, *Phys. Rev. Lett.* **37**, 1059–1062 (1976).
- [17] A. Poniewierski and T.J. Sluckin, *Liq. Cryst.* **2**, 281–311 (1987).
- [18] K. Kočevár, A. Borštnik, I. Mušević and S. Žumer, *Phys. Rev. Lett.* **86**, 5914–5917 (2001).
- [19] R. van Roij, M. Dijkstra and R. Evans, *Europhys. Lett.* **49**, 350–356 (2000).
- [20] R. van Roij, M. Dijkstra and R. Evans, *J. Chem. Phys.* **113**, 7689–7701 (2000).
- [21] I.C. Gârlea and B.M. Mulder, *Soft Matter* **11**, 608–614 (2015).
- [22] V.A. Ivanov, A.S. Rodionova, J.A. Martemyanova, M.R. Stukan, M. Müller, W. Paul and K. Binder, *Journal of Chemical Physics* **138**, 234903 (2013).
- [23] H. Reich and M. Schmidt, *J. Phys: Cond. Matt.* **19**, 326103 (2007).
- [24] J.Z. Chen, *Progress in Polymer Science* **54–55**, 3–46 (2016).
- [25] S. Ye, P. Zhang and J.Z.Y. Chen, *Soft Matter* **12**, 2948–2959 (2016).
- [26] D.A. Luzhbin and Y.L. Chen, *Macromolecules* **49**, 6139–6147 (2016).
- [27] Z. Dogic and S. Fraden, in , edited by G. Gompper and M. Schick (, , 2007), Vol. 2, Chap. Phase Behavior of Rod-Like Viruses and Virus-Sphere Mixtures, 1st ed., pp. 1–86.
- [28] Z. Dogic and S. Fraden, *Langmuir* **16**, 7820–7824 (2000).
- [29] M.J. Zakhary, P. Sharma, A. Ward, S. Yardimici and Z. Dogic, *Soft Matter* **9**, 8306–8313 (2013).
- [30] E. Grelet, *Phys. Rev. Lett.* **100**, 168301 (2008).
- [31] D. Guu, J.K.G. Dhont, G.A. Vliegenthart and M.P. Lettinga, *J. Phys: Condens. Matt.* **24**, 464101 (2012).
- [32] E. Barry, D. Beller and Z. Dogic, *Soft Matter* **5**, 2563–2570 (2009).
- [33] M.P. Lettinga and E. Grelet, *Phys. Rev. Lett.* **99** (2007).
- [34] D. Bartolo, G. Degré, P. Nghe and V. Studer, *Lab Chip* **8**, 274–279 (2008).
- [35] T. Troppenz, A. Kuijk, A. Imhof, A. van Blaaderen, M. Dijkstra and R. van Roij, *Phys. Chem. Chem. Phys.* **17**, 22423–22430 (2015).
- [36] R. Zwanzig, *J. Chem. Phys.* **39**, 1714–1721 (1963).
- [37] S.A. Egorov, A. Milchev, P. Virnau and K. Binder, *Journal of Chemical Physics* **144**, 174902 (2016).
- [38] H. Fynewer and A. Yethiraj, *J. Chem. Phys.* **108**, 1636 (1998).